Available online at www.sciencedirect.com

ScienceDirect

journal homepage: www.elsevier.com/locate/he

Low-carbon scheduling of integrated hydrogen transport and energy system

*Yaowen Yu**, *Yue Chen*, *Jianhua Jiang*, *Yuanzheng Li*

Belt and Road Joint Laboratory on Measurement and Control Technology, School of Artificial Intelligence and Automation, Huazhong University of Science and Technology, Wuhan 430074, China

HIGHLIGHTS

- Emission-operation optimization of Integrated Hydrogen Transport and Energy System.
- The timeliness of hydrogen deliveries is modeled with delays penalized.
- The scheduling problem is formulated as a mixed-integer linear programming problem.

ARTICLE INFO

Article history:
Received 16 January 2023
Received in revised form
15 March 2023
Accepted 5 April 2023
Available online 27 April 2023

Keywords:
Hydrogen supply chain network
Hydrogen energy
Integrated transport and energy system
Mixed-integer linear programming
Tube trailer

ABSTRACT

The joint consideration of hydrogen supply chain networks and electric power systems can promote hydrogen-fueled transportation and the penetration of renewable energy. This paper develops a low-carbon scheduling approach for an Integrated Hydrogen Transport and Energy System (IHTES). To reduce carbon emissions, the environmental cost from the hydrogen supply chain network and electric power system is jointly minimized with the operational cost of IHTES. To consider the timeliness of hydrogen deliveries, hydrogen transport via tube trailers is innovatively modeled as an extended vehicle routing problem with time windows, and delays are penalized. The scheduling problem is formulated as a mixed-integer linear programming problem so that it can be efficiently solved using the branch-and-cut method. Case studies illustrate and validate the proposed model, and demonstrate the computational efficiency of our approach. Carbon emissions are reduced by 47.8% when the emission cost is co-optimized with the operational cost. The operational cost of the hydrogen supply chain network is reduced by 7.3% when the timeliness of hydrogen deliveries is modeled.

Introduction

Greenhouse gas emissions, particularly carbon dioxide (CO_2), cause climate change, including global warming and extreme weather events. Consequently, it has garnered global attention to reduce CO_2 emissions.

On the one hand, carbon capture and storage technologies, such as biomass and biochar carbon materials, have emerged to reduce CO_2 emissions from fossil fuel combustions [1], especially at coal-fired thermoelectric power plants [2,3]. On the other hand, as a clean and flexible energy carrier, hydrogen has been regarded worldwide as a fuel for the future [4] and is promising for emission reductions in transportation

Abbreviations: HFS, Hydrogen Fueling Station; HPS, Hydrogen Production Station; HS, Hydrogen Station (HFS and HPS); IHTES, Integrated Hydrogen Transport and Energy System; MILP, Mixed-integer linear programming; PV, photovoltaic.

* *Corresponding author.*
E-mail address: yaowen_yu@hust.edu.cn (Y. Yu).

https://doi.org/10.1016/j.ijhydene.2023.04.064
0360-3199/

Nomenclature

Indexes and Sets

b	Index of nodes, $1 \le b \le N_b$
d	Index of tube trailer, $1 \le d \le N_d$
g	Index of thermal generators, $1 \le g \le N_g$
i (or j)	Index of HSs, $1 \le i, j \le N_{HS}$
k	Index of HPSs, $1 \le k \le N_{HPS}$
l	Index of transmission lines, $1 \le l \le N_l$
r	Index of renewable energy resources, $1 \le r \le N_r$
t	Index of time (hours), $1 \le t \le N_t$
T	Index of trailer scheduling periods, $1 \le T \le N_T$
$\alpha(l)$, $\beta(l)$	From and to nodes of transmission line l, respectively
$\varphi(d)$	HPS where trailer d sets out
$\Phi^G(b)$	Set of thermal generators at node b
$\Phi^{Re}(b)$	Set of renewable energy resources at node b
$\Phi^{HPS}(b)$	Set of HPSs at node b
$\Phi^{Tr}(k)$	Set of trailers setting out from HPS k
$\Phi^{Sc}(T)$	Set of hours in scheduling period T

Parameters

C_g	Generation and maintenance cost coefficient of generator g ($/MWh)
C_g^{SU}, C_g^{SD}	Startup and shutdown cost coefficients of generator g, respectively ($)
C_g^{NL}	No-load cost coefficient of generator g ($)
C^{Dr}	Fixed payment to each hydrogen trailer if scheduled for one period ($)
C_r^{Re}	Operation and maintenance cost coefficient of renewable energy resource r ($/MWh)
C^R	Routing cost coefficient of trailers ($/km)
C^P	Penalty cost coefficient for delay ($/h)
C^{Em}	Cost coefficient of carbon emission ($/kg)
e^G	Carbon emission coefficient of generators (kg/MWh)
e^{Tr}	Carbon emission coefficient of trailers (kg/km)
$\overline{f}_l$	Capacity of transmission line l at time t (MW)
$m_{i,T}^D$	Hydrogen demand of HFS i in period T (kg)
$\overline{m}_k^{HPS}$	Maximal hydrogen produced at HPS k (kg)
$\overline{m}_d^{Tr}$	Maximal hydrogen loaded to trailer d (kg)
M	A big number
$p_{b,t}^D$	Electric demand at node b at time t (MW)
$\underline{P}_g$, $\overline{P}_g$	Minimal and maximal power outputs of generator g, respectively (MW)
$\widehat{p}_{r,t}^{Re}$	Predicted electric power output of renewable energy resource r at time t (MW)
q_k^{Im}	Limit of hydrogen imported into storage at HPS k (kg)
q_k^{Ex}	Limit of hydrogen exported from storage at HPS k (kg)
$\underline{Q}_i^{HFS}$, $\overline{Q}_i^{HFS}$	Minimal and maximal hydrogen storage limits at HFS i, respectively (kg)
$\underline{Q}_k^{HPS}$, $\overline{Q}_k^{HPS}$	Minimal and maximal hydrogen storage limits at HPS k, respectively (kg)
$R_{i,j}$	Distance between HS i and HS j (km)
$u_{i,T}$	The latest delivery time required by HFS i in period T (h)
v_d	Speed of hydrogen trailer d (km/h)
X_l	Reactance of line l (Ω)
Δ_g	Ramp rate of generator g (MW/h)
κ	Electricity-to-hydrogen conversion rate (kg/MWh)

Variables and functions

$f_{l,t}$	Power flow along transmission line l at time t (MW)
$p_{g,t}^G$	Electric power output of thermal generator g at time t (MW)
$p_{k,t}^H$	Electric power utilized by HPS k (MW)
$p_{r,t}^{Re}$	Electric power output of renewable energy resource r at time t (MW)
$q_{k,t}$	Net hydrogen imported into storage at HPS k at time t (kg)
$Q_{k,t}^{HPS}$	Hydrogen stored at HPS k at time t (kg)
$Q_{i,T}^{HFS}$	Hydrogen stored at HFS k in period T (kg)
$m_{d,i,T}^{HFS}$	Hydrogen transported to HFS i from trailer d in period T (h)
$m_{k,t}^{HPS}$	Hydrogen produced at HPS k at time t (kg)
$m_{d,T}^{Tr}$	Hydrogen loaded to trailer d in period T (kg)
n_T	Number of trailers scheduled during period T
$s_{d,i,T}$	Delivery time when trailer d arrives at HFS i in period T (h)
$w_{d,i,T}$	Delay caused by trailer d if not arriving at HFS i on time in period T (h)
$x_{d,i,j,T}$	Binary decision indicating whether trailer d travels from station i to j in period T, with "1" representing yes and "0" otherwise
$y_{g,t}^{SU}$	Binary startup decision of generator g at time t, with "1" representing starting up and "0" otherwise
$y_{g,t}^{SD}$	Binary shutdown decision of generator g at time t, with "1" representing the shutting down and "0" otherwise
$z_{g,t}$	Binary commitment decision of generator g at time t, with "1" representing online and "0" offline
$\theta_{b,t}$	Voltage phase angle at node b at time t
F^{Dr}	Labor cost of trailer drivers ($)
F^{El}	Operational cost of the electric power grid ($)
F^{Em}	Cost of carbon emission ($)
F^H	Operational cost of the hydrogen supply chain network ($)
F^P	Penalty cost for delay ($)
F^R	Routing cost ($)

and industrial applications that are difficult to decarbonize [5,6].

Hydrogen can be produced via electrolysis using excess electricity generated from wind and solar energies. It can be stored as a high-pressure gas or liquid, and then transformed with oxygen into electricity by fuel cells [7]. In the transportation sector, fuel cells are a well-known alternative to replace internal combustion engines using fossil fuels in cars, trucks, buses, trains, ships, and airplanes [8]. For instance, a solar-driven self-sufficient integrated hydrogen energy system with a proton exchange membrane (PEM) fuel cell was developed for caravan applications [9]. Hybrid configurations based on fuel cells and batteries were investigated as auxiliary power units for chemical tanker vessels [10].

The existing literature on hydrogen energy systems considers on-site or remote hydrogen production. In on-site hydrogen production, hydrogen production, storage, and consumption occur at the same location, without involving hydrogen transport [11–14]. Wind and solar energies were used to power the aqueous electrolysis of native biomass to produce hydrogen for an on-site hydrogen fueling station (HFS) [11]. An off-grid solar-based charging station integrated with hydrogen energy was developed and assessed [12]. An off-grid charging station was designed for electric and hydrogen vehicles, where solar panels were used to satisfy the electrical demand and power the water electrolyzer for hydrogen production [13]. Although on-site hydrogen production can reduce the cost and complexity of hydrogen transport, its capacity may not be sufficient to satisfy the increasing demand for hydrogen energy, particularly in urban areas with space and security concerns or locations without sufficient renewable energy [15,16].

In remote hydrogen production, hydrogen is transported [17] via pipelines [18–21], tube trailers [15,22–24], or both [25,26]. To avoid a large investment in the construction of new hydrogen pipelines, hydrogen was mixed with natural gas and transported through existing gas pipelines [18–20]. Various ratios of H_2 in the mixed gas was considered, and the most economical percentage of H_2 was found to be 10% in summer and 18% in winter, respectively, considering the gas quality and security [18]. Compared with pipelines, tube trailers are generally the simplest method for infrastructure requirements because well-constructed roads can be utilized [16,23]. Moreover, the hydrogen loss and cost of compression are low for tube trailers [16].

Recently, an integrated scheduling model was developed for the joint consideration of the hydrogen supply chain network and electric power system with hydrogen transported via tube trailers [22]. The model contained an extended vehicle routing problem to minimize the cost of hydrogen delivery with trailers and coordinated hydrogen production, storage, and transportation with renewable energy in an electric power system. Furthermore, the demand response of hydrogen fuel cell vehicles was considered [15]. The joint consideration of the hydrogen supply chain network and electric power system can reduce the total operational cost, increase renewable energy penetration, and improve the resource allocation efficiency [15,22].

The following research gaps are discovered:

First, it is crucial to explicitly consider carbon emissions in hydrogen-related energy systems to effectively reduce the carbon footprint [27–32]. However, recent integrated studies of hydrogen supply chain networks with tube trailers and electric power systems [15,22] primarily focused on operational cost minimization, whereas the cost associated with carbon emissions has rarely been considered.

Second, the timeliness of hydrogen delivery to each HFS is not considered. Since hydrogen demands from different HFSs may have different priorities, it is more realistic to consider their requirements for hydrogen delivery times.

To bridge these gaps, this paper develops a low-carbon scheduling approach for an Integrated Hydrogen Transport and Energy System (IHTES) with the following major contributions:

- The environmental cost of carbon emissions from the hydrogen supply chain network and electric power system is jointly minimized with the operational cost of IHTES.
- To consider the timeliness of hydrogen deliveries, hydrogen transport via tube trailers is modeled as an extended vehicle routing problem with time windows, and delays are penalized.
- The scheduling problem is formulated as a mixed-integer linear programming (MILP) problem so that it can be efficiently solved using the branch-and-cut method.

Furthermore, case studies illustrate and validate the proposed model, and demonstrate the computational efficiency of our approach.

Low-carbon scheduling approach for IHTES

This section presents the proposed scheduling approach. Subsection Overview of the scheduling problem provides an overview of the IHTES. Subsection Hydrogen transport model formulates the hydrogen transport model that considers the timeliness of hydrogen deliveries. Subsections (HFS model)–(Electric power system model) describe models of the HFS, the HPS, and the electric power system, respectively. Subsection Objective function describes the objective function that minimizes the total operational and environmental cost. The scheduling problem is formulated as an MILP problem. Subsection Solution algorithm solves the problem using the branch-and-cut method.

Overview of the scheduling problem

Based on [22], the IHTES considered in this paper is illustrated in Fig. 1. The hydrogen supply chain network comprises HFSs, HPSs, roads, and tube trailers that transport hydrogen from HPSs to HFSs in each scheduling period. The scheduling period is the work shift of the tube trailer drivers. The number of tube trailers to dispatch during each period and their routes are to be determined.

The network is coupled with the electric power grid via HPSs, where electric power, especially from renewable energy resources, can be utilized to produce hydrogen using electrolyzers. Moreover, the system-wide and generator constraints in the power grid should be satisfied.

Carbon emissions may originate from both transport and energy systems. The objective function is to minimize the total operational and environmental cost of IHTES.

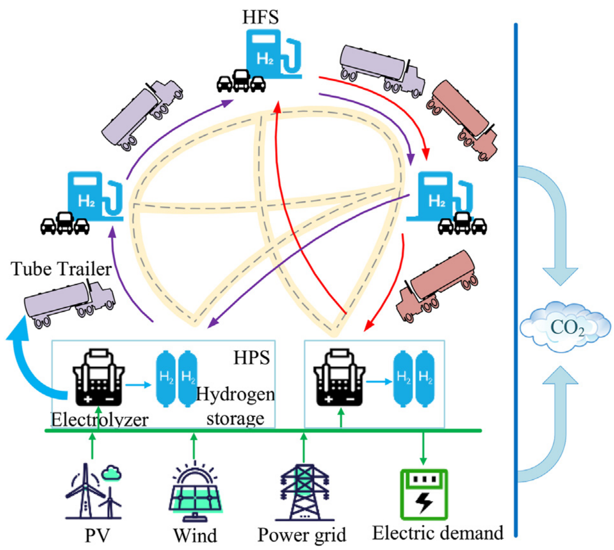

Fig. 1 – Structure of the IHTES

Building on recent studies [15,22], the constraints and objective function of the proposed low-carbon scheduling model are presented as follows.

Hydrogen transport model

To consider the timeliness of hydrogen deliveries, hydrogen transport via tube trailers is modeled here as an extended vehicle routing problem with time windows [33–35].

To ensure the validity of routes, trailer d leaving station i can reach one station at most in scheduling period T, i.e.,

$$\sum_{j \in HS} x_{d,i,j,T} \leq 1, \forall d, \forall i, \forall T. \tag{1}$$

Note that there are two situations in which the left-hand side is equal to 0. If i is an HPS, (1) means that trailer d stays at the current HPS i in scheduling period T. If i is an HFS, (1) indicates that trailer d has not reached HFS i in period T.

Moreover, to ensure the continuity of routes, in scheduling period T, trailer d that arrives at hydrogen station j should also leave j, i.e.,

$$\sum_{i \in HS} x_{d,i,j,T} = \sum_{i \in HS} x_{d,j,i,T}, \forall d, \forall j, \forall T. \tag{2}$$

If trailer d is scheduled, its hydrogen loaded in period T should not exceed the maximal value; otherwise, it will not be loaded, i.e.,

$$0 \leq m^{Tr}_{d,T} \leq \overline{m}^{Tr}_{d} \cdot \sum_{j \in HRS} x_{d,\varphi(d),j,T}, \forall d, \forall T. \tag{3}$$

In scheduling period T, the hydrogen loaded onto all trailers from HPS k should be equal to the hydrogen produced in this period minus the net hydrogen imported into storage at this HPS, i.e.,

$$\sum_{d \in \Phi^{Tr}(k)} m^{Tr}_{d,T} = \sum_{t \in \Phi^{Sc}(T)} \left(m^{HPS}_{k,t} - q_{k,t} \right), \forall k, \forall T. \tag{4}$$

In scheduling period T, if trailer d goes from station i to station j, then the arrival time of hydrogen station j is the arrival time at station i plus the routing time of the trailer; if trailer d does not visit i or j, such a temporal relationship is not applicable. Generally, a temporal relationship involving the logic condition is expressed using the Big M method [35]:

$$s_{d,i,T} + R_{i,j} / v_d - M \cdot \left(1 - x_{d,i,j,T}\right) \leq s_{d,j,T}, \forall d, \forall i, \forall j, \forall T. \tag{5}$$

Moreover, the above constraints can avoid sub-loops of trailer d in scheduling period T.

The arrival (delivery) time of trailer d at HFS i in period T should not be later than the corresponding latest delivery time required by HFS i, i.e.,

$$s_{d,i,T} - w_{d,i,T} \leq u_{i,T}, \forall d, \forall i, \forall T, \tag{6}$$

where $w_{d,i,t}$ is a non-negative slack variable that softens each constraint and represents the delay.

HFS model

The hydrogen stored (in hydrogen tanks) at HFS i in period T is the value in period $T-1$ plus the hydrogen transported minus the hydrogen consumption of the HFS, i.e.,

$$Q^{HFS}_{i,T} = Q^{HFS}_{i,T-1} + \sum_{d}^{N_d} m^{HFS}_{d,i,T} - m^{D}_{i,T}, \forall i, \forall T. \tag{7}$$

The hydrogen in HFS i in period T should be within its upper and lower limits, i.e.,

$$\underline{Q}^{HFS}_{i} \leq Q^{HFS}_{i,T} \leq \overline{Q}^{HFS}_{i}, \forall i, \forall T. \tag{8}$$

The hydrogen transported to all HFSs from trailer d in period T equals the hydrogen loaded to this trailer, i.e.,

$$\sum_{i \in HFS} m^{HFS}_{d,i,T} = m^{Tr}_{d,T}, \forall d, \forall T. \tag{9}$$

However, if trailer d has not reached HFS j during this period, the hydrogen transported to HFS j from this trailer must be zero. This condition can be expressed as follows:

$$0 \leq m^{HFS}_{d,j,T} \leq \overline{m}^{Tr}_{d} \cdot \sum_{i \in HS} x_{d,i,j,T}, \forall j, \forall d, \forall T. \tag{10}$$

Note that $\overline{m}^{Tr}_{d}$ is essentially used as Big M in constraints (10) given (3) and (9).

HPS model

The conversion from electricity to hydrogen is calculated by the following equation:

$$\kappa \cdot p^{H}_{k,t} = m^{HPS}_{k,t}, \forall k, \forall t, \tag{11}$$

where the electricity-to-hydrogen conversion rate κ also takes the electricity consumption for hydrogen compression at a certain pressure level into consideration.

The hydrogen produced at HPS k at time t should be within zero and its maximal value, i.e.,

$$0 \leq m^{HPS}_{k,t} \leq \overline{m}^{HPS}_{k}, \forall k, \forall t. \tag{12}$$

The hydrogen stored at HPS k at time t is the value at time $t-1$ plus the net hydrogen imported into storage at time t, i.e.,

$$Q^{HPS}_{k,t} = Q^{HPS}_{k,t-1} + q_{k,t}, \forall k, \forall t, \tag{13}$$

where the net hydrogen imported into storage $q_{k,t}$ equals the hydrogen imported minus the hydrogen exported.

The stored hydrogen and net imported hydrogen should be within their corresponding limits, i.e.,

$$\underline{Q}^{HPS}_{k} \leq Q^{HPS}_{k,t} \leq \overline{Q}^{HPS}_{k}, \forall k, \forall t, \tag{14}$$

$$-q^{Ex}_{k} \leq q_{k,t} \leq q^{Im}_{k}, \forall k, \forall t. \tag{15}$$

Electric power system model

The power balance constraint on node b at hour t is the output power of the thermal generators and renewable energy resources on this node minus the electricity demand, and the electric power consumed by the HPSs is equal to the total outflow of the node minus the total inflow, i.e.,

$$\sum_{g \in \Phi^{G}(b)} p^{G}_{g,t} + \sum_{r \in \Phi^{Re}(b)} p^{Re}_{r,t} - p^{D}_{b,t} - \sum_{k \in \Phi^{HPS}(b)} p^{H}_{k,t} = \sum_{l:\alpha(l)=b} f_{l,t} - \sum_{l:\beta(l)=b} f_{l,t}, \forall b, \forall t. \tag{16}$$

Constraints of generators are from the unit commitment problem [36]:

$$z_{g,t}\underline{P}_{g} \leq p^{G}_{g,t} \leq z_{g,t}\overline{P}_{g}, \forall g, \forall t, \tag{17}$$

$$-\Delta_{g} \leq p^{G}_{g,t} - p^{G}_{g,t-1} \leq \Delta_{g}, \forall g, \forall t, \tag{18}$$

$$z_{g,t} - z_{g,t-1} = y^{SU}_{g,t} - y^{SD}_{g,t}, \forall g, \forall t. \tag{19}$$

Constraints (17) are generator capacity constraints, and constraints (18) are ramp rate constraints. The relationship among commitment, startup, and shutdown decisions is expressed in (19).

The output power of renewable energy resource r at hour t should be within zero and its predicted value at this hour, i.e.,

$$0 \leq p^{Re}_{r,t} \leq \widehat{p}^{Re}_{r,t}, \forall r, \forall t. \tag{20}$$

The solar/wind power is curtailed when its output power is less than the predicted value.

For transmission lines, the transmission capacity constraints with DC power flow calculated using the voltage phase angles [37] are provided below:

$$-\overline{f}_{l} \leq f_{l,t} = \frac{\theta_{\alpha(l),t} - \theta_{\beta(l),t}}{X_{l}} \leq \overline{f}_{l}, \forall l, \forall t. \tag{21}$$

Objective function

The objective function is to minimize the total operational and environmental cost of the IHTES.

$$\min F = F^{H} + F^{El} + F^{Em}, \tag{22}$$

where F^{H} (\$) denotes the operational cost of the hydrogen supply chain network, F^{El} (\$) denotes the operational cost of the electric power grid, and F^{Em} (\$) denotes the cost of the carbon emissions.

The operational cost of the hydrogen supply chain network includes the labor cost of trailer drivers F^{Dr} (\$), routing cost F^{R} (\$), and penalty cost for delay F^{P} (\$), i.e.,

$$F^{H} = F^{Dr} + F^{R} + F^{P}. \tag{23}$$

The labor cost is the total fixed payment to all scheduled hydrogen trailers for their scheduled periods, i.e.,

$$F^{Dr} = C^{Dr}\sum_{T}^{N_T} n_{T}, \tag{24}$$

where n_T indicates the number of trailers scheduled in period T and can be calculated as the total number of trailers leaving all hydrogen production stations,

$$n_{T} = \sum_{k \in HPS}\sum_{d \in \Phi_3(k)}\sum_{i \in HRS} x_{d,k,i,T}, \forall T. \tag{25}$$

The routing cost is based on distances traveled by trailers:

$$F^{R} = C^{R}\sum_{T}^{N_T}\sum_{d}^{N_d}\sum_{i}^{N_{HS}}\sum_{j}^{N_{HS}} R_{i,j}x_{d,i,j,T}. \tag{26}$$

The penalty cost for delay is calculated when trailers do not arrive on time:

$$F^{P} = C^{P}\sum_{T}^{N_T}\sum_{d}^{N_d}\sum_{i}^{N_{HFS}} w_{d,i,T}. \tag{27}$$

The operational cost of the electric power system is the sum of the generation and maintenance, no-load, startup, and shutdown costs of all generators, plus the operation and maintenance of renewable energy resources, i.e.,

$$F^{El} = \sum_{g}^{N_g}\sum_{t}^{N_t}\left(C_{g}p^{G}_{g,t} + C^{NL}_{g}z_{g,t} + C^{SU}_{g}y^{SU}_{g,t} + C^{SD}_{g}y^{SD}_{g,t}\right) + \sum_{r}^{N_r}\sum_{t}^{N_t} C^{Re}_{r}p^{Re}_{r,t}. \tag{28}$$

Notably, the depreciation of generators and renewable energy resources in the long term can be considered in the corresponding maintenance costs. The depreciation of the electrolyzers and other hydrogen-related devices can be considered similarly and are not modeled here for simplicity.

The cost of carbon emissions entails the emission cost from generators and that from trailers, i.e.,

$$F^{Em} = C^{Em}\left(e^{G}\sum_{g}^{N_g}\sum_{t}^{N_t} p^{G}_{g,t} + e^{Tr}\sum_{T}^{N_T}\sum_{d}^{N_d}\sum_{i}^{N_{HS}}\sum_{j}^{N_{HS}} R_{i,j}x_{d,i,j,T}\right). \tag{29}$$

The aforementioned low-carbon scheduling model of the IHTES is formulated as an MILP problem. The total operational and environmental cost is minimized by coordinating the hydrogen supply chain network and electric power system. Since renewable power generation with zero emissions is promoted in co-optimization, solar/wind curtailment is not directly penalized in the objective function.

Solution algorithm

The above MILP problem can be solved using the branch-and-cut method [38,39], which synergistically combines the branch-and-bound and cutting-plane methods. The branch-and-bound algorithm solves a series of linear programming relaxations as lower bounds of the MILP problem for intelligent enumeration of possible candidate solutions in a search tree. Cutting planes are constraints added to the model to eliminate non-integer solutions, and can generally reduce the number of branches in the branch-and-bound search tree. The branch-and-cut method guarantees the optimality and has been applied to solve various MILP problems. Commercial solvers containing the branch-and-cut method, such as Gurobi [38] and CPLEX [39], make it convenient to solve various MILP problems.

Moreover, for computational efficiency, the Big M in constraints (5) should be selected properly to shrink the search space of the branch-and-cut method. If the value of M is too big, the linear programming relaxations may not be able to provide useful lower bounds for the algorithm. Based on (5), the following inequality should hold,

$$M \geq s_{d,i,T} - s_{d,j,T} + R_{i,j}/v_d,\ \forall d,\ \forall i,\ \forall j,\ \forall T. \tag{30}$$

As a result, the minimum valid value of M should be the maximum value of the right-hand-side of (30), which can be obtained as follows,

$$\max\left(s_{d,i,T} - s_{d,j,T} + R_{i,j}\,/\,v_d\right) = \left|\Phi^{Sc}(T)\right| + \max\left(R_{i,j}\,/\,v_d\right), \tag{31}$$

where $|\Phi^{Sc}(T)|$ is the number of hours in scheduling period T. With properly selected values of the Big M, the MILP low-carbon scheduling problem can be efficiently solved.

Case studies

In this section, case studies are presented to illustrate and validate the proposed model, and demonstrate the computational efficiency of our approach.

Testing system and enviroment

The testing system comprised a modified IEEE 6-node electric power system [40] and a hydrogen supply chain network with two HPSs and six HFSs, as shown in Fig. 2. The optimization horizon contains 24 h and three scheduling periods. Scheduling Period 1 is from Hour 6 (5:00–5:59) to Hour 11, Period 2 from Hour 12 to Hour 17, and Period 3 from Hour 18 to Hour 23.

The total electricity demand with an hourly pattern for a winter weekday from the IEEE RTS-96 system [41] is shown in Fig. 3. A PV power plant is added to Node 5, and a wind farm is added to Node 3. Hourly PV and wind generation data from Ref. [42] are shown in Figs. 4 and 5, respectively. The operation and maintenance cost coefficients of PV and wind are \$4.69/MWh and \$9.38/MWh, respectively [43]. The parameters of the generators in Ref. [40] are listed in Table 1. The parameters of the HPSs and HFSs based on [22] are presented in Tables 2 and 3, respectively. The hydrogen demands of the HFSs for the three periods are illustrated in Fig. 6. The latest delivery times required by the HFSs are listed in Table 4. Trailers 1, 2 and 3 depart from HPS 1, and Trailers 4, 5 and 6 depart from HPS 2. The speed of all trailers is 30 km/h. The electricity-to-hydrogen conversion rate of each HPS considering the

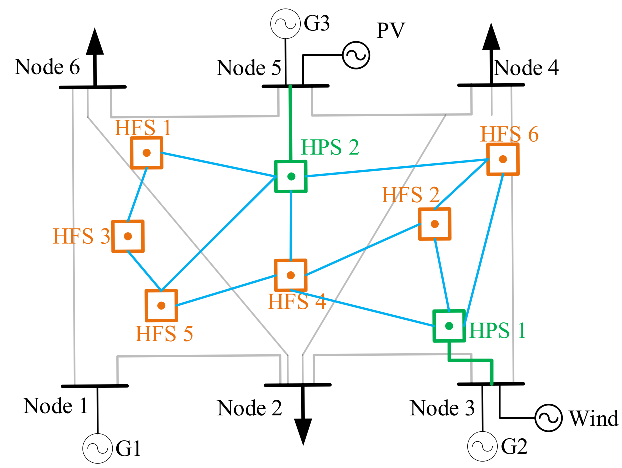

Fig. 2 – Topology of the testing system.

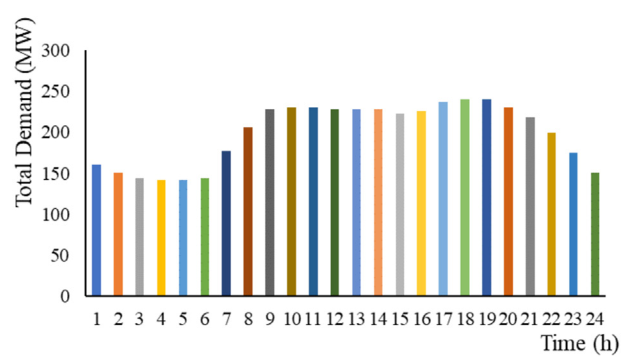

Fig. 3 – Hourly electricity demand curve.

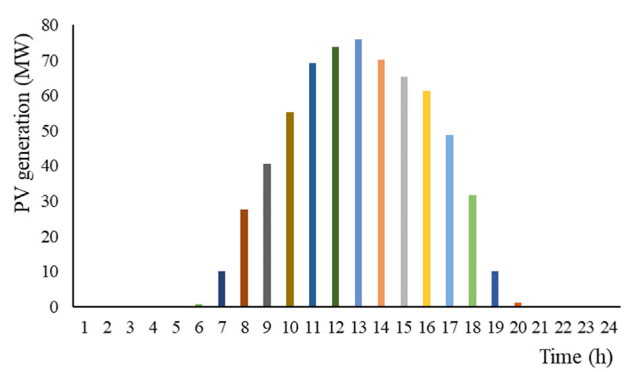

Fig. 4 – Hourly PV generation curve.

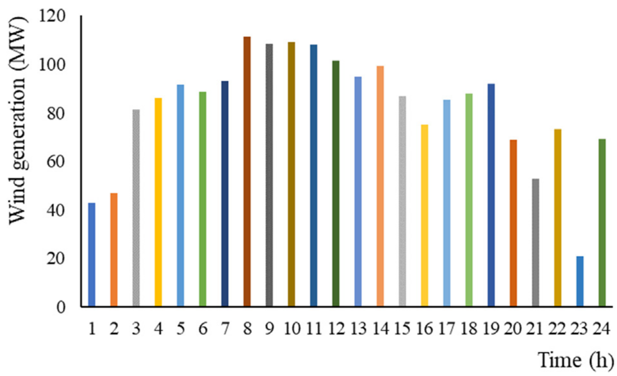

Fig. 5 – Hourly wind generation curve.

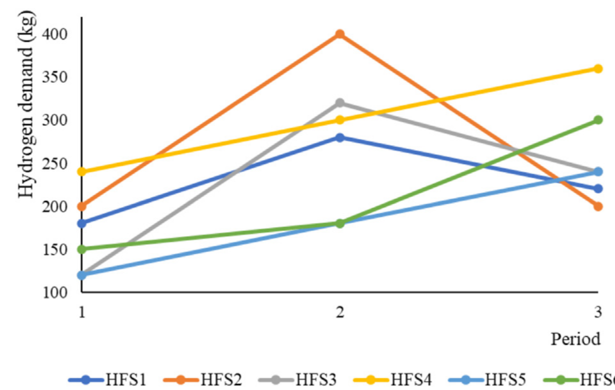

Fig. 6 – Hydrogen demand curves of HFSs.

Table 1 – Generator parameters.

Generator	Node	Minimal power output (MW)	Maximal power output (MW)
G1	1	20	150
G2	3	50	200
G3	5	100	300

Generator	Ramp rate (MW/h)	Generation and maintenance cost ($/MWh)	Startup/shutdown cost ($)	No-load cost ($)
G1	50	7.38	173	50
G2	40	6.85	412	40
G3	15	5.61	60	60

Table 2 – HPS parameters.

HPS	Minimum hydrogen level (kg)	Maximum hydrogen level (kg)	Limit of hydrogen imported (kg)	Limit of hydrogen exported (kg)
1	200	1200	1200	1200
2	400	1600	1600	1600

Table 3 – HFS parameters.

HFS	Minimum hydrogen level (kg)	Maximum hydrogen level (kg)
1	100	600
2	300	1000
3	200	600
4	100	600
5	150	800
6	120	600

Table 4 – Latest delivery times required by HFSs.

	HFS 1	HFS 2	HFS 3
Period 1	6: 30	6: 00	6: 20
Period 2	12: 20	12: 40	12: 30
Period 3	18: 50	18: 30	19: 00
	HFS 4	**HFS 5**	**HFS 6**
Period 1	6: 00	6: 30	6: 30
Period 2	13: 30	13: 30	11: 50
Period 3	19: 00	19:30	19: 45

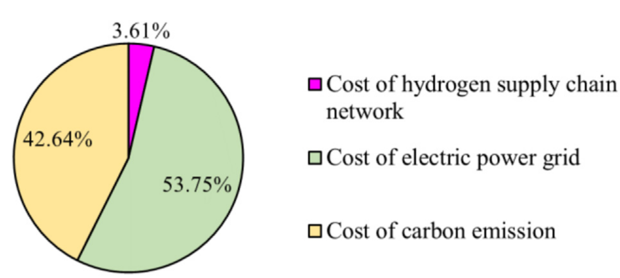

Fig. 7 – Pie chart of costs.

electricity consumption for hydrogen compression at a certain pressure level is 16.46 kg/MWh. The routing cost coefficient of the tube trailers is $6.5/km. The penalty cost coefficient for delay is $300/h.

The carbon emission coefficient of the generators is 572 kg/MWh [44], and the carbon emission coefficient of tube trailers is 0.12 kg/km [27]. The cost coefficient of carbon emissions is $0.024/kg [44].

Our scheduling model is implemented in Python and solved using Gurobi 9.0.3 [38]. The relative mixed-integer programming gap required to stop the algorithm is 0.01%. Numerical experiments are conducted on a PC with a 6-core 12-thread i5-10400 CPU at 2.90 GHz and 16 GB of memory.

Results and illustration of our model

In the optimal solution, the total cost is $69,687.88. The operational cost of the hydrogen supply chain network is $2514.48 (3.61% of the total cost), the operational cost of the electric power grid is $37,460.2 (53.75%), and the cost of carbon emissions is $29,713.2 (42.64%), with a total carbon emission of 1.238×10^6 kg. A pie chart of the costs is shown in Fig. 7.

The power output curves of generators are plotted in Fig. 8. It appears that G3 is offline for all hours because its ramp rate is too small to satisfy the intertemporal volatility of electricity

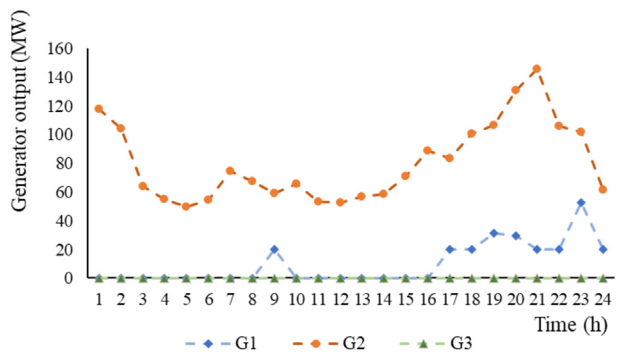

Fig. 8 – Power output curves of generators.

and hydrogen demands. G2 is online for all hours since it has a relatively large ramp rate, the smallest no-load cost among the three generators, and a lower generation and maintenance cost than G1. G1 appears to be online at Hour 9 and from Hours 17 to 24.

The optimal number of scheduled tube trailers and routing paths for each scheduling period are listed in Table 5. There are three trailers scheduled for Period 1, two for Period 2, and one for Period 3. Since hydrogen can be stored in HFSs, more hydrogen is delivered in earlier periods to reduce the labor and routing costs of transporting hydrogen in later periods.

Consider Period 2 as an example, one tube trailer sets out from HPS 1, visits HFSs 4, 2 and 6, and finally returns to HPS 1. From the topology in Fig. 2, it can be observed that HFS 2 is much closer to HPS 1 than to HPS 2, so HFS 2 is supplied by HPS 1. HFS 4 (or 6) has similar distances from HPS1 and from HPS 2, so HFS 4 (or 6) can be supplied by either HPS. Another tube trailer sets out from HPS 2, visits HFSs 5, 3 and 1, and then returns to HPS 2. HFSs 1, 3 and 5 are much closer to HPS 2 than to HPS 1, so they are all supplied by HPS 2.

The delivery times of the tube trailers are presented in Table 6. Evidently, all HFSs are delivered on time. Consider Trailer 1 in Period 2 as an example: It can be observed that the order and times of delivering HFSs 4, 2, and 6 are consistent with the latest delivery times required in Table 4.

Effect of emission cost

The effectiveness of considering the emission cost in the objective function is validated. The costs and carbon emissions considering the emission cost are compared with the corresponding values without considering the emission cost in Table 7.

Evidently, although the total operational cost without considering the emission cost is lower than that considering the emission cost, the total cost, $87,428.36, is much higher than $69,687.88 with a co-optimized emission cost. The reason is that 2.371×10^6 kg of carbon emissions are produced at an emission cost of $56,905.68 when the emission cost is not

Table 5 – Scheduled number of tuber trailers and routing paths.

Scheduling period	No. of trailers	Scheduled routes
1	3	HPS1→HFS2→HFS6→HPS1, HPS2→HFS4→HFS5→HPS2, HPS2→HFS1→HFS3→HPS2
2	2	HPS1→HFS4→HFS2→HFS6→HPS1, HPS2→HFS5→HFS3→HFS1→HPS2
3	1	HPS2→HFS6→HPS2

Table 6 – Results of delivery times.

Scheduling period	Trailer	Delivery time
1	1	HFS2:5:13; HFS6: 5:27
	4	HFS4: 5:16; HFS5:5:31
	5	HFS1: 5:18; HFS3:5:34
2	1	HFS4: 11:20; HFS2: 11:38; HFS6: 11:52
	4	HFS5: 11:24; HFS3: 11:37; HFS1: 11:53
3	4	HFS6: 17:25

Table 7 – Comparison of costs and carbon emissions.

	W/o emission cost	With emission cost
Total cost ($)	87,428.36	69,687.88
Total operational cost ($)	30,522.68	39,974.68
F^{El} ($)	28,008.2	37,460.2
F^{H} ($)	2514.48	2514.48
F^{Em} ($)	56,905.68	29,713.2
Carbon emission (kg)	2.371×10^6	1.238×10^6

Table 8 – Tight latest delivery times required by HFSs.

	HFS 1	HFS 2	HFS 3
Period 1	6: 30	6: 00	5: 30
Period 2	11: 40	11: 30	12: 00
Period 3	18: 30	18: 30	19: 00
	HFS 4	HFS 5	HFS 6
Period 1	6: 30	6: 00	6: 30
Period 2	11: 24	11: 24	11: 30
Period 3	19: 00	19: 00	18: 00

considered in the optimization, and the carbon emissions are reduced by 47.8% when the emission cost is co-optimized.

Effect of hydrogen delivery timeliness

It turns out that the latest delivery times required by HFSs in Table 4 are loose, so the results are the same with or without considering the timeliness of hydrogen deliveries in the hydrogen transport model.

To validate the effectiveness of modeling the hydrogen delivery timeliness, another tight delivery-time scenario with the latest delivery times required by the HFSs provided in Table 8 is also tested.

When the timeliness of hydrogen deliveries is not modeled, the results remain the same as those in Tables 5 and 6 It can be observed that in Scheduling Period 1, Trailer 3 is late at HFS 3 by 4 min. In Scheduling Period 2, Trailer 1 is late at HFSs 2 and 6 by eight and 22 min, respectively, and Trailer 2 is late at HFS1 by 13 min.

When the timeliness of hydrogen deliveries is modeled, the optimal number of scheduled tube trailers and routing paths for each scheduling period are listed in Table 9, and the delivery times of the tube trailers are listed in Table 10. It can be observed that delay only occurs in Scheduling Period 2, in which Trailer 2 is late at HFS 5 by 7 min.

The costs and carbon emissions with and without modeling the timeliness of hydrogen deliveries are compared in Table 11. Although the total cost of the entire IHTES system is only reduced slightly by modeling the timeliness, the operational cost of the hydrogen supply chain network considering the penalty cost for delay is reduced by 7.3%. The reason is that the penalty cost is reduced from \$235 to \$35 when the timeliness is modeled.

Table 11 – Comparison of delivery times in the tight delivery-time scenario.

	W/o timeliness	With timeliness
Total cost (\$)	69922.88	69848.2
Total operational cost (\$)	40,209.68	40110.04
F^{El} (\$)	37,460.2	37,472.7
F^{H} (\$)	2749.48	2637.34
Penalty cost (\$)	235	35
F^{Em} (\$)	29,713.2	29,738.16
Carbon emission (kg)	1.238×10^6	1.239×10^6

Effect of different fossil fuel prices

To investigate the impacts of different fossil fuel prices on scheduling solutions, the cost coefficients of generators (in Table 1) are doubled to mimic a scenario when fossil fuel prices increase, and are cut into half to mimic another scenario when fossil fuel prices decrease.

At double generator costs, the total cost is \$85618.88. At half the generator costs, the total cost is \$61722.48. Pie charts in Fig. 9 illustrate the breakdown of these costs. It appears that at double generator costs, the operational cost of the electric power grid increases to 62.36% of the total cost, compared to 53.75% in Fig. 7. The cost percentages of the hydrogen supply chain network and carbon emissions decrease. The opposite situation can be observed at half the generator costs.

Computational efficiency of our approach

The MILP model with the testing system has 2911 rows, 3069 columns including 1749 continuous variables and 1320 integer variables, and 10,699 non-zeros.

Table 9 – Scheduled number of tuber trailers and routing paths in the tight delivery-time scenario.

Scheduling period	No. of trailers	Scheduled routes
1	3	HPS1→HFS6→HFS2→HPS1, HPS2→HFS5→HFS4→HPS2, HPS2→HFS3→HFS1→HPS2
2	2	HPS1→HFS2→HFS6→HPS1, HPS2→HFS4→HFS5→HFS3→HPS2
3	1	HPS2→HFS6→HFS4→HFS1→HPS2

Table 10 – Results of delivery times in the tight delivery-time scenario.

Scheduling period	Trailer	Delivery time
1	1	HFS6:5:24; HFS2: 5:38
	4	HFS5: 5:24; HFS4:5:39
	5	HFS3: 5:25; HFS1:5:41
2	1	HFS2: 11:13; HFS6: 11:27
	4	HFS4: 11:16; HFS5: 11:31; HFS3: 11:43
3	4	HFS6: 17:25; HFS4: 17:56; HFS1: 18:23

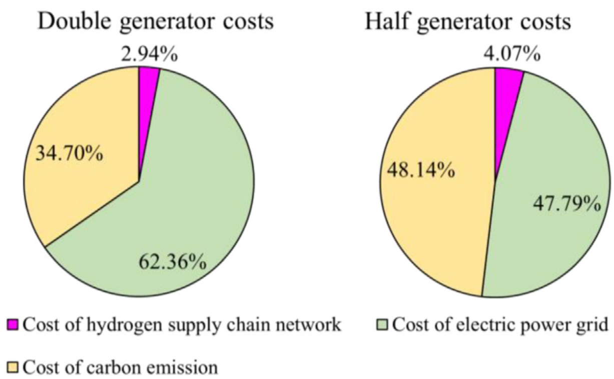

Fig. 9 – Results of different generation costs.

Table 12 – Computational performance results.

Big M	Total cost ($)	Solution time (s)	No. of nodes
7	69,687.88	12.75	17,619
70	69,687.88	17.46	21,655
700	69,687.88	18.16	26,612

The minimum valid value of the Big M in (5) can be calculated as 6.92 (hour) based on (31). Consequently, the value of 7 is selected as a proper choice for the Big M. Larger values of 70 and 700 are also tested for comparison. Computational performance results of our approach with different Big M values are summarized in Table 12.

For all valid Big M values, the total costs are the same, $69,687.88. It takes 12.75, 17.46, and 18.16 s to solve the scheduling problem with 7, 70, and 700 as the Big M, respectively. In other words, the properly selected Big M value in the MILP scheduling problem can reduce the solution time by 29.8% (= (18.16–12.75)/18.16). The reason is that a smaller Big M value can tighten the MILP formulation to reduce the number of nodes that need to be explored by the branch-and-cut method.

Conclusion

This paper develops a low-carbon scheduling approach for IHTES. The total operational and environmental cost is minimized. Hydrogen transport via tube trailers is modeled as an extended vehicle routing problem with time windows, and delays are penalized. The scheduling problem is formulated as an MILP problem so that it can be efficiently solved using the branch-and-cut method. Case studies illustrate and validate the proposed model, and demonstrate the computational efficiency of our approach.

The main results of this paper are as follows:

- Carbon emissions are reduced by 47.8% when the emission cost is co-optimized with the operational cost compared to the operational cost optimization without emission cost.
- The operational cost of the hydrogen supply chain network considering the penalty cost for delay is reduced by 7.3% when the timeliness of hydrogen deliveries is modeled.
- The MILP scheduling problem with the properly selected Big M value can reduce the solution time by 29.8%.

This study sheds light on the modeling and solution of complicated coupling networks. Future research directions include the explicit modeling of renewable uncertainty through stochastic programming [15,22], robust optimization [40,45], or interval optimization [36] to improve the accuracy and security of scheduling strategies under high penetrations of renewables. Moreover, data-driven machine learning methods may be used to further improve the computational efficiency.

Declaration of competing interest

The authors declare that they have no known competing financial interests or personal relationships that could have appeared to influence the work reported in this paper.

Acknowledgement

This work was supported by the National Natural Science Foundation of China (62203181).

References

[1] Karimi M, Shirzad M, Silva JAC, Rodrigues AE. Biomass/Biochar carbon materials for CO2 capture and sequestration by cyclic adsorption processes: a review and prospects for future directions. J CO2 Util 2022;57:101890.
[2] Akbari-Dibavar A, Mohammadi-Ivatloo B, Zare K, Khalili T, Bidram A. Economic-emission dispatch problem in power systems with carbon capture power plants. IEEE Trans Ind Appl 2021;57(4):3341–51.
[3] Karimi M, Rahimpour MR, Rafiei R, Shariati A, Iranshahi D. Improving thermal efficiency and increasing production rate in the double moving beds thermally coupled reactors by using differential evolution (DE) technique. Appl Therm Eng 2016;94:543–58.
[4] Bragatto T, Bucarelli MA, Carere F, Cavadenti A, Santori F. Optimization of an energy district for fuel cell electric vehicles: cost scenarios of a real case study on a waste and recycling fleet. Int J Hydrogen Energy 2022;47(95):40156–71.
[5] Bødal EF, Mallapragada D, Botterud A, Korpås M. Decarbonization synergies from joint planning of electricity and hydrogen production: a Texas case study. Int J Hydrogen Energy 2020;45(58):32899–915.
[6] Zhao Y, Liu Q, Duan Y, Zhang Y, Cui Y, Huang Y, Gao D, Shi L, Wang J, Yi Q. Hydrogen energy deployment in decarbonizing transportation sector using multi-supply-demand integrated scenario analysis with nonlinear programming - a Shanxi case study. Int J Hydrogen Energy 2022;47(44):19338–52.
[7] Thomas JM, Edwards PP, Dobson PJ, Owen GP. Decarbonising energy: the developing international activity in hydrogen technologies and fuel cells. J Energy Chem 2020;51:405–15.

[8] Pramuanjaroenkij A, Kakaç S. The fuel cell electric vehicles: the highlight review. Int J Hydrogen Energy 2023;48(25):9401–25.
[9] Karaca AE, Dincer I. Development and evaluation of a solar based integrated hydrogen energy system for mobile applications. Energy Convers Manag 2023;280:116808.
[10] Korkmaz SA, Erginer KE, Yuksel O, Konur O, Colpan CO. Environmental and economic analyses of fuel cell and battery-based hybrid systems utilized as auxiliary power units on a chemical tanker vessel. Int J Hydrogen Energy 2023. https://doi.org/10.1016/j.ijhydene.2023.01.320. Available online.
[11] Zhang K, Zhou B, Wing S, Li C, Chung C, Voropai N. Optimal coordinated control of multi-renewable-to-hydrogen production system for hydrogen fueling stations. IEEE Trans Ind Appl 2022;58(2):2728–39.
[12] Erdemir D, Dincer I. Development of solar-driven charging station integrated with hydrogen as an energy storage option. Energy Convers Manag 2022;257:115436.
[13] Mehrjerdi H. Off-grid solar powered charging station for electric and hydrogen vehicles including fuel cell and hydrogen storage. Int J Hydrogen Energy 2019;44(23):11574–83.
[14] Lin H, Wu Q, Chen X, Yang X, Guo X, Lv J, Lu T, Song S, McElroy M. Economic and technological feasibility of using power-to-hydrogen technology under higher wind penetration in China. Renew Energy 2021;173:569–80.
[15] Dong W, Shao C, Feng C, Bie Z, Wang X. Cooperative operation of power and hydrogen energy systems with HFCV demand response. IEEE Trans Ind Appl 2022;58(2):2630–9.
[16] Moradi R, Groth KM. Hydrogen storage and delivery: review of the state of the art technologies and risk and reliability analysis. Int J Hydrogen Energy 2019;44(23):12254–69.
[17] Demir ME, Dincer I. Cost assessment and evaluation of various hydrogen delivery scenarios. Int J Hydrogen Energy 2018;43(22):10420–30.
[18] Fu C, Lin J, Song Y, Li J, Song J. Optimal operation of an integrated energy system incorporated with HCNG distribution networks. IEEE Trans Sustain Energy 2020;11(4):2141–51.
[19] Zhao P, Lu X, Cao Z, Gu C, Ai Q, Liu H, Bian Y, Li S. Volt-VAR-pressure optimization of integrated energy systems with hydrogen injection. IEEE Trans Power Syst 2021;36(3):2403–15.
[20] Zhao P, Gu C, Cao Z, Hu Z, Zhang X, Chen X, Hernando-Gil I, Ding Y. Economic-effective multi-energy management with voltage regulation networked with energy hubs. IEEE Trans Power Syst 2021;36(3):2503–15.
[21] Gan W, Yan M, Yao W, Guo J, Fang J, Ai X, Wen J. Multi-network coordinated hydrogen supply infrastructure planning for the integration of hydrogen vehicles and renewable energy. IEEE Trans Ind Appl 2022;58(2):2875–86.
[22] Shao C, Feng C, Shahidehpour M, Zhou Q, Wang X, Wang X. Optimal stochastic operation of integrated electric power and renewable energy with vehicle-based hydrogen energy system. IEEE Trans Power Syst 2021;36(5):4310–21.
[23] Yang G, Jiang Y, You S. Planning and operation of a hydrogen supply chain network based on the off-grid wind-hydrogen coupling system. Int J Hydrogen Energy 2020;45(41):20721–39.
[24] Ban M, Bai W, Song W, Zhu L, Xia S, Zhu Z, Wu T. Optimal scheduling for integrated energy-mobility systems based on renewable-to-hydrogen stations and tank truck fleets. IEEE Trans Ind Appl 2022;58(2):2666–76.
[25] He G, Mallapragada DS, Bose A, Heuberger CF, Gençer E. Hydrogen supply chain planning with flexible transmission and storage scheduling. IEEE Trans Sustain Energy 2021;12(3):1730–40.
[26] Seo S-K, Yun D-Y, Lee C-J. Design and optimization of a hydrogen supply chain using a centralized storage model. Appl Energy 2020;262:114452.
[27] Zhou L, Zhang F, Wang L, Zhang Q. Flexible hydrogen production source for fuel cell vehicle to reduce emission pollution and costs under the multi-objective optimization framework. J Clean Prod 2022;337:130284.
[28] Wei X, Zhang X, Sun Y, Qiu J. Carbon emission flow oriented tri-level planning of integrated electricity–hydrogen–gas system with hydrogen vehicles. IEEE Trans Ind Appl 2022;58(2):2607–17.
[29] AlHajri I, Ahmadian A, Elkamel A. Techno-economic-environmental assessment of an integrated electricity and gas network in the presence of electric and hydrogen vehicles: a mixed-integer linear programming approach. J Clean Prod 2021;319:128578.
[30] Sun G, Li G, Li P, Xia S, Zhu Z, Shahidehpour M. Coordinated operation of hydrogen-integrated urban transportation and power distribution networks considering fuel cell electric vehicles. IEEE Trans Ind Appl 2022;58(2):2652–65.
[31] Song Y, Mu H, Li N, Wang H. Multi-objective optimization of large-scale grid connected photovoltaic-hydrogen-natural gas integrated energy power station based on carbon emission priority. Int J Hydrogen Energy 2023;48(10):4087–103.
[32] Zhang C, Greenblatt JB, Wei M, Eichman J, Saxena S, Muratori M, Guerra OJ. Flexible grid-based electrolysis hydrogen production for fuel cell vehicles reduces costs and greenhouse gas emissions. Appl Energy 2020;278:115651.
[33] Kim G, Ong YS, Heng C, Tan P, Zhang N. City vehicle routing problem (city VRP): a review. IEEE Trans Intell Transport Syst 2015;16:1654–66.
[34] Lu D, Gzara F. The robust vehicle routing problem with time windows: solution by branch and price and cut. Eur J Oper Res 2019;275:925–38.
[35] Ramos TRP, Gomes MI, Póvoa APB. Multi-depot vehicle routing problem: a comparative study of alternative formulations. Int J Logist Res Appl 2020;23(2):103–20.
[36] Yu Y, Luh PB, Litvinov E, Zheng T, Zhao J, Zhao F, Schiro D A. Transmission contingency-constrained unit commitment with high penetration of renewables via interval optimization. IEEE Trans Power Syst 2017;32(2):1410–21.
[37] Yu Y, Luh PB. Scalable corrective security-constrained economic dispatch considering conflicting contingencies. Int J Electr Power Energy Syst 2018;98:269–78.
[38] Gurobi optimization. https://www.gurobi.com/; 2021.
[39] IBM ILOG CPLEX Optimization. https://www.ibm.com/cn-zh/analytics/cplex-optimizer.
[40] Wang Q, Watson J-P, Guan Y. Two-stage robust optimization for N-k contingency-constrained unit commitment. IEEE Trans Power Syst 2013;28(3):2366–75.
[41] Grigg C. The IEEE reliability test system-1996: a report prepared by the reliability test system task force of the application of probability methods subcommittee. IEEE Trans Power Syst 1999;14(3):1010–20.
[42] Eskom. Eskom solar insolation data. http://www.eskom.co.za/AboutElectricity/RenewableEnergy/Pages/Solar_Information.aspx.

[43] Zhang C, Liu X, He X, Li C. The output optimization of multi-microgrids connected to distribution network during peak, flat and valley periods. In: The 6th IEEE PES asia-pacific power and energy engineering conference. Hong Kong: Kowloon; 2014.

[44] Liu J, Chen X, Yang H, Shan K. Hybrid renewable energy applications in zero-energy buildings and communities integrating battery and hydrogen vehicle storage. Appl Energy 2021;290:116733.

[45] Wang Y, Kazemi M, Nojavan S, Jermsittiparsert K. Robust design of off-grid solar-powered charging station for hydrogen and electric vehicles via robust optimization approach. Int J Hydrogen Energy 2020;45(38):18995–9006.